



Published in final edited form as:

Acc Chem Res. 2020 May 19; 53(5): 1056–1065. doi:10.1021/acs.accounts.0c00044.

Developing Scaling Relationships for Molecular Electrocatalysis through Studies of Fe-Porphyrin-Catalyzed O₂ Reduction

Daniel J. Martin[§],

Department of Chemistry, Yale University, New Haven, Connecticut 06520, United States

Catherine F. Wise[§],

Department of Chemistry, Yale University, New Haven, Connecticut 06520, United States

Michael L. Pegis,

Department of Chemistry, Massachusetts Institute of Technology, Cambridge, Massachusetts 02139, United States

James M. Mayer

Department of Chemistry, Yale University, New Haven, Connecticut 06520, United States

CONSPECTUS:

The oxygen reduction reaction (ORR) is a multiproton/multielectron transformation in which dioxygen (O₂) is reduced to water or hydrogen peroxide and serves as the cathode reaction in most fuel cells. The ORR (O₂ + 4e⁻ + 4H⁺ → 2H₂O) involves up to nine substrates and thus requires navigating a complicated reaction landscape, typically with several high-energy intermediates. Many catalysts can perform this reaction, though few operate with fast rates and at low overpotentials (close to the thermodynamic potential). Attempts to optimize these parameters, both in homogeneous and heterogeneous electrocatalytic systems, have focused on modifying catalyst design and understanding kinetic/thermodynamic relationships between catalytic intermediates. One such method for analyzing and predicting catalyst reactivity and efficiency has been the development of “molecular scaling relationships”. Here, we share our experience deriving and utilizing molecular scaling relationships for soluble, iron-porphyrin-catalyzed O₂ reduction in organic solvents. These relationships correlate turnover frequencies (TOF_{max}) and effective overpotentials (η_{eff}), properties uniquely defined for homogeneous catalysts. Following a general introduction of scaling relationships for both homogeneous and heterogeneous electrocatalysis, we describe the components of such scaling relationships: (i) the overall thermochemistry of the reaction and (ii) the rate and rate law of the catalyzed reaction. We then show how connecting these thermodynamic and kinetic parameters reveals *multiple* molecular scaling relationships for iron-porphyrin-catalyzed O₂ reduction. For example, the log(TOF_{max}) responds steeply to changes in η_{eff} that result from different catalyst reduction potentials (18.5 decades in TOF_{max}/V in η_{eff}) but much less dramatically to changes in η_{eff} that arise from varying the pK_a of the acid buffer (5.1 decades in TOF_{max}/V in η_{eff}). Thus, a single scaling relationship is not always sufficient for describing molecular electrocatalysis. This is particularly evident when the catalyst identity and

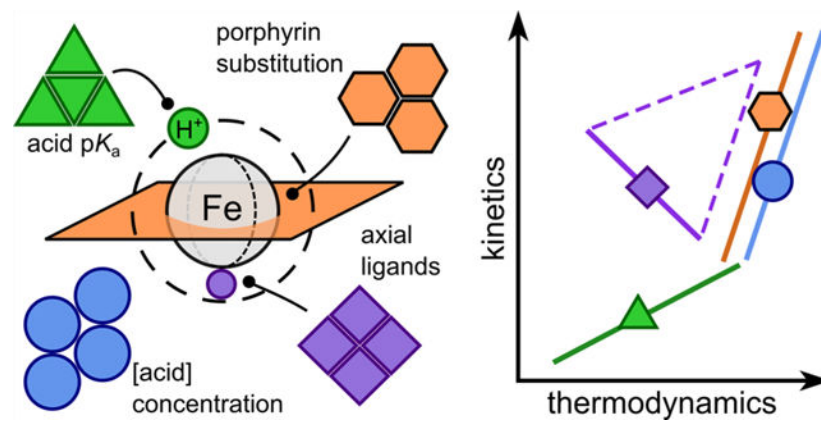
Corresponding Author james.mayer@yale.edu.

[§]D.J.M. and C.F.W. contributed equally.

The authors declare no competing financial interest.

reaction conditions are coupled. Using these multiple scaling relationships, we demonstrate that the metrics of turnover frequency and effective overpotential can be predictably tuned to achieve faster rates at lowered overpotentials. This Account uses a collection of related stories describing our research on soluble iron-porphyrin-catalyzed ORR to show how molecular scaling relationships can be derived and used for any electrocatalytic reaction. Such scaling relationships are powerful tools that connect the thermochemistry, mechanism, and rate law for a catalytic system. We hope that this collection shows the utility and simplicity of the molecular scaling approach for understanding catalysis, for enabling direct comparisons between catalyst systems, and for optimizing catalytic processes.

Graphical Abstract



I. INTRODUCTION

The reduction of dioxygen (O₂) to water (H₂O) is a critical chemical transformation for many biological and artificial energy systems, such as cellular respiration and fuel cell technologies.^{1–3} For energy applications, the four-electron/four-proton (4e⁻/4H⁺) reduction of O₂ to H₂O (eq 1) is preferred over the less exoergic 2e⁻/2H⁺ reduction of O₂ to hydrogen peroxide (H₂O₂).



Performing the 4e⁻/4H⁺ oxygen reduction reaction (ORR) at high rates and close to its thermodynamic potential (e.g., at low *overpotentials*) is a major challenge.^{1,4–6} The best systems use platinum-group-metal catalysts, but improved replacements with earth-abundant materials are required for next-generation energy technologies.⁴ Many of the fundamental aspects of this challenge are more amenable to study with homogeneous molecular ORR electrocatalysts, though soluble catalysts are less likely to be the technological solution.^{7,8} Research on molecular electrocatalysts provides new strategies for efficient catalysis of the ORR and other proton/electron energy-conversion reactions.

This Account describes how our studies of soluble iron porphyrin ORR catalysts (Fe(por)) in organic solvents led us to develop “molecular scaling relationships”. These relationships

reveal how the primary metrics of catalysis (turnover frequency and overpotential) depend on the components of the catalytic system. Using ORR electrocatalysis by iron porphyrins as a case study, we develop the thermodynamic and kinetic parameters relevant to molecular electrocatalysis and then derive the corresponding molecular scaling relationships. We demonstrate how catalysis depends not only on catalyst identity but also on the buffer and the medium. These quantitative relationships provide a powerful new way to understand, compare, and improve multiproton/multielectron electrocatalytic systems. We hope that this Account will stimulate our readers to use this approach for their catalytic applications.

II. METRICS FOR HOMOGENEOUS MOLECULAR ELECTROCATALYSIS

Molecular electrocatalysis involves soluble catalysts, often in nonaqueous media, that are driven by the exchange of electrons with an electrode. The primary scientific metrics that describe a catalytic system—defined as both the electrocatalyst and its surrounding medium—are rates, over potentials, selectivity, and robustness. Emphasized here are the parameters of maximum turnover frequency (TOF_{max}), or moles of product per mole of catalyst (in the reaction diffusion layer) per second, and effective overpotential (η_{eff} , see below).^{9,10} With this emphasis, the “best” catalyst is the one that attains the highest TOF_{max} at the lowest η_{eff} .

Cyclic voltammetry is the technique most often used to evaluate molecular electrocatalysis, where TOF_{max} is obtained by analyzing the response of the electrocatalyst in the presence and absence of substrate (blue and black curves in Figure 1).¹¹ In an ideal system, the catalytic current reaches a maximum at potentials beyond $E_{\text{cat}/2}$,^{11,12} where it is limited by chemical steps in the solution.^{13,14} For nonideal voltammograms, foot-of-the-wave analysis (FOWA) is often used to extract TOF_{max} from the “foot” of the catalytic wave.^{11,13} The η_{eff} is defined as the difference between $E_{\text{cat}/2}$ and the thermodynamic potential of the reaction of interest under catalytic conditions (E_{rxn} ; eq 2).^{9,10} In Fe(por)-catalyzed ORR, $E_{\text{cat}/2}$ is equivalent to the iron(III)/iron(II) reduction potential, $E_{1/2}(\text{Fe}^{\text{III}}/\text{Fe}^{\text{II}})$, and E_{rxn} is the ORR equilibrium potential under the reaction conditions, $E_{\text{O}_2/\text{H}_2\text{O}}$ (eq 3).^{10–12,15}

$$\eta_{\text{eff}} = E_{\text{rxn}} - E_{\text{cat}/2} \quad (2)$$

$$\eta_{\text{eff}} = E_{\text{O}_2/\text{H}_2\text{O}} - E_{1/2}(\text{Fe}^{\text{III}}/\text{Fe}^{\text{II}}) \quad (3)$$

III. STANDARD AND EQUILIBRIUM POTENTIALS

The thermodynamic potential of a catalyzed reaction is needed to determine η_{eff} .^{9,10} Until recently, however, the standard potentials were not known for ORR or many other multiproton/multielectron reactions in organic solvents. Building on Roberts and Bullock’s seminal work,¹⁶ Roberts, Appel, and our laboratory developed a method to estimate such potentials from the aqueous standard potential and the nonaqueous standard hydrogen potential ($E^{\circ}_{\text{H}^+/\text{H}_2}$; collected from open-circuit potential measurements in the organic solvent of interest containing an acid/base buffer of known $\text{p}K_{\text{a}}$) using a thermochemical cycle (Scheme 1).¹⁷ This approach has been used to determine the standard potentials for

reductions of O₂, CO₂, and N₂ to various products in acetonitrile (MeCN) and dimethylformamide (DMF).^{17,18}

$$E_{\text{O}_2/\text{H}_2\text{O}} = E_{\text{O}_2/\text{H}_2\text{O}}^\circ - \frac{2.303RT}{4F} \log \left(\frac{[\text{H}_2\text{O}]^2 [\text{A}^-]^4}{P_{\text{O}_2} [\text{HA}]^4} \right) - (0.0592 \text{ V}) \text{p}K_{\text{a}} \quad (4)$$

The *equilibrium* potential under catalytic conditions (E_{rxn}) almost always differs from the standard potential because standard-state conditions (e.g., [H₂O] = 1 M) are almost never used. The equilibrium potential is given by the Nernst equation (eq 4 for the ORR), which includes the concentrations or pressures of all species involved and the acid p*K*_a. To determine E_{rxn} , we strongly recommend that catalytic solutions be buffered with 1:1 acid (HA) and conjugate base (A⁻).^{12,19,20} If only HA is present, then the [A⁻] at the electrode is not known, and $E_{\text{O}_2/\text{H}_2\text{O}}$ is undefined. Additionally, homoconjugation of acids and their conjugate bases in organic media (AH...A⁻) can strongly affect the [HA]/[A⁻] ratio unless their concentrations are equal.^{12,19,20}

The methods described in this section allow for straightforward determination of the thermodynamic efficiencies of molecular catalysis for many proton-coupled electron transfer (PCET) reactions. We encourage authors to take advantage of these approaches so that they may report η_{eff} in addition to TOF_{max} in their studies.

IV. SCALING RELATIONSHIPS 1: IDENTIFYING CORRELATIONS

Using the above approaches, we determined kinetic (TOF_{max}) and thermodynamic (η_{eff}) values for many Fe(por) ORR catalysts under different conditions. Analysis of these data showed linear correlations between log(TOF_{max}) and η_{eff} (eq 5, Figure 2A).¹⁰ Such correlations between kinetic and thermodynamic parameters have often been used to derive structure/activity relationships for molecular electrocatalysts.^{10,21–23} Correlations using TOF_{max} values are not quite linear free energy relationships (LFERs), because TOF_{max} values depend on reaction conditions. However, changes in log(TOF_{max}) are linear with changes in G^\ddagger as long as the reaction conditions do not change (eq 7). Most importantly, normal LFERs correlate a rate parameter with the free energy *for that particular step*. Thus, TOF_{max} values generally should not correlate with the *overall* reaction energetics η_{eff} , which cover many steps. In fact, there are multiple log(TOF_{max})/ η_{eff} correlations, as described below.

$$\log(\text{TOF}_{\text{max}}) = m(\eta_{\text{eff}}) + C \quad (5)$$

$$k = (\kappa k_{\text{b}} T / h) \exp(-\Delta G^\ddagger / RT) \quad (6)$$

$$\Delta \log(\text{TOF}_{\text{max}}) = -\Delta(\Delta G^\ddagger / RT) \quad (7)$$

Plotting $\log(\text{TOF}_{\text{max}})$ vs η_{eff} is the simplest way to compare the efficiencies of a set of molecular electrocatalytic systems (Figure 2), where each $(\eta_{\text{eff}}, \log(\text{TOF}_{\text{max}}))$ point describes a catalytic system. The closer these points are to the top-left corner of the plot, the better the system (lower overpotentials, faster rates).^{21,24,25} For instance, the points at the top right of Figure 2A represent spectacularly rapid ORR catalysts (TOF_{max} values $>10^6 \text{ s}^{-1}$, the fastest known), yet the high rates come at a cost of high overpotentials ($\eta_{\text{eff}} > 1.2 \text{ V}$)¹⁰. Similar trade-offs in $\log(\text{TOF}_{\text{max}})/\eta_{\text{eff}}$ are observed for other electrocatalysts and reactions. For example, the scaling relationships in Figure 2A for 11 different Fe(por) ORR catalysts resemble those in Figure 2B for hydrogen evolution electrocatalysis by nickel phosphine–amine complexes.²⁶ The different slopes of the lines in Figure 2B indicate that the catalytic TOF_{max} varies in different ways depending on how η_{eff} is changed (see sections VI–VIII).

The scaling relationships common to heterogeneous electrocatalysis are also kinetic/thermodynamic relationships,^{5,6} but they are otherwise quite different from the molecular examples above. Heterogeneous scaling relationships typically correlate current density at a given overpotential with a single relevant scaling “descriptor” chosen by the researcher. Thermochemical descriptors such as the surface–H or surface–OH bond strengths are common, because they are both relevant to catalytic steps and relatively easy to compute.^{5,6} The heterogeneous analysis assumes that the free energies of the important intermediates all scale with the descriptor (the “scaling” relationship). Plots of rate vs descriptor frequently show a “volcano” shape, where the peak position can provide valuable predictions for a particular mechanism (see ref 27 regarding criticisms of this approach)^{5,28,29}

In contrast, the next section shows that molecular electrocatalysts often have more complex mechanisms, in which electrons and protons are often added in separate steps. The subsequent sections (VI–VIII) then bring together these tools and results to understand ORR catalysis by soluble iron porphyrins, and to thereby develop the more complex molecular scaling relationships that correlate TOF_{max} and η_{eff} .

V. THE MECHANISM OF O₂ REDUCTION BY IRON PORPHYRINS IN NONAQUEOUS SOLVENTS

Deriving $\log(\text{TOF}_{\text{max}})/\eta_{\text{eff}}$ relationships for molecular electrocatalysts relies on knowing the catalytic rate law. This section describes our parallel electrochemical and spectroscopic studies of O₂ reduction catalyzed by iron tetraphenylporphyrin, Fe(TPP), as a case study.³⁰ In acidified, anaerobic DMF, voltammograms of Fe(TPP) showed a reversible Fe^{III}/Fe^{II} redox couple.^{30,31} Upon saturating the solution with O₂, a large, irreversible current appeared, centered over $E_{1/2}(\text{Fe}^{\text{III}}/\text{Fe}^{\text{II}})$ (Figure 3A). The shape of the voltammogram suggested an EC' mechanism, where rapid, reversible ET was followed by irreversible chemical step(s).¹¹ From such voltammograms, TOF_{max} values were calculated using foot-of-the-wave analysis (FOWA).^{13,32} The variation of TOF_{max} with reaction conditions showed that the reaction was first-order in $[\text{Fe}(\text{TPP})]$, $[\text{O}_2]$, and $[\text{acid}]$ and yielded the third-order rate constant, k_{cat} (eqs 8 and 9).^{30,31}

$$\frac{d[\text{O}_2]}{dt} = k_{\text{cat}}[\text{HA}][\text{O}_2][\text{Fe}(\text{TPP})] \quad (8)$$

$$\text{TOF}_{\text{max}} = k_{\text{cat}}[\text{HA}][\text{O}_2] \quad (9)$$

The rate law indicated an ORR mechanism of initial electron transfer (ET) to form $\text{Fe}^{\text{II}}(\text{TPP})$, pre-equilibrium O_2 -binding to form the iron-superoxo complex, $\text{Fe}^{\text{III}}(\text{TPP})(\text{O}_2^{\bullet-})$, and rate-limiting protonation of $\text{Fe}^{\text{III}}(\text{TPP})(\text{O}_2^{\bullet-})$ (Figure 4).³⁰ To probe the underlying thermochemistry of these intermediates, we examined both equilibrium and catalytic ORR reactions using decamethylferrocene (Fc^*) as the terminal reductant and *p*-toluene sulfonic acid (*p*TsOH) as the acid.

The thermodynamics of the two pre-equilibrium steps—ET and O_2 binding—were measured directly using variable-temperature UV–vis spectroscopy. For example, addition of O_2 to $\text{Fe}^{\text{II}}(\text{TPP})$ showed reversible formation of $\text{Fe}^{\text{III}}(\text{TPP})(\text{O}_2^{\bullet-})$ (Figure 3C). Van 't Hoff analyses of the derived equilibrium constants for ET (K_{ET}) and O_2 binding (K_{O_2}) yielded the H^\ddagger and S^\ddagger for both steps.³⁰

The catalytic reaction was monitored by variable-temperature optical stopped-flow, combining a solution of $[\text{Fe}^{\text{III}}(\text{TPP})]\text{OTf}$, O_2 , and *p*TsOH with a solution of Fc^* (Figure 3B). Globally fitting the kinetic data using COPASI³³ gave thermochemical parameters for the ET and O_2 pre-equilibria that agreed with the values obtained from the van 't Hoff analyses, providing strong evidence for the proposed mechanism. The derived rate constants showed a significant activation barrier for proton transfer (PT). Computations revealed that much of this barrier stemmed from the requisite formation of a preassociation complex involving an acid molecule, DMF solvent, and $\text{Fe}^{\text{III}}(\text{TPP})(\text{O}_2^{\bullet-})$. Under conditions where $\text{Fe}^{\text{II}}(\text{TPP})$ is the predominant catalyst resting state, $k_{\text{cat}} = K_{\text{O}_2}k_{\text{PT}}$; thus, changes to either (or both) of these terms will impact TOF_{max} .³⁰

VI. SCALING RELATIONSHIPS 2: EFFECTS OF CATALYST $E_{1/2}$ AND BUFFER $\text{p}K_{\text{a}}$ ON $\text{Fe}(\text{por})$ -CATALYZED O_2 REDUCTION

The mechanistic conclusions provided a more quantitative understanding of the relationship between $\log(\text{TOF}_{\text{max}})$ and η_{eff} . The variation in TOF_{max} is due to changes in G^\ddagger , which is (under most conditions) the sum of the free energy for pre-equilibrium O_2 binding ($\Delta G^\circ_{\text{O}_2}$) and the barrier for protonation (G^\ddagger_{PT}) of $\text{Fe}^{\text{III}}(\text{por})(\text{O}_2^{\bullet-})$ by exogenous acid (eq 10, Figure 5).³⁰ $\Delta G^\circ_{\text{O}_2}$ depends on the catalyst, and G^\ddagger_{PT} is well approximated via the Bronsted law, as a fraction (α) of the PT driving force, G°_{PT} . G°_{PT} is, in turn, given by the difference in $\text{p}K_{\text{a}}$ between the acid and $\text{Fe}^{\text{III}}(\text{TPP})(\text{O}_2^{\bullet-})$ (eq 11). Values of $\Delta G^\circ_{\text{O}_2}$ and G°_{PT} are therefore influenced by intrinsic properties of the catalyst system, namely, the catalyst $E_{1/2}$ and buffer $\text{p}K_{\text{a}}$. Changes in the overpotential are described by eq 3 above,

$$\eta_{\text{eff}} = E_{\text{O}_2/\text{H}_2\text{O}} - E_{1/2}(\text{Fe}^{\text{III}}/\text{Fe}^{\text{II}}).$$

$$\Delta G^\ddagger = \Delta G^\circ_{O_2} + \Delta G^\ddagger_{PT} \quad (10)$$

$$\begin{aligned} \Delta G^\ddagger_{PT} &= \alpha \Delta G^\circ_{PT} \\ &= \alpha 2.303 [pK_a(\text{HA}) - pK_a\{\text{Fe}^{\text{III}}(\text{por})(\text{O}_2^{\bullet -})\}] \end{aligned} \quad (11)$$

Effect of Catalyst $E_{1/2}$

The empirical scaling line in Figure 2A corresponds to systems in which only $E_{1/2}$ was varied. Changes in $E_{1/2}$ do not shift the ORR equilibrium potential; thus, $\Delta\eta_{\text{eff}} = -\Delta E_{1/2}$. In terms of TOF_{max} , changes in $E_{1/2}$ affect both $\Delta G^\circ_{O_2}(K_{O_2})$ and the pK_a of the superoxide complex (eq 12).

A quantitative understanding of the effects of $E_{1/2}$ on TOF for Fe(por)-catalyzed ORR required computational determination of pK_{O_2} and $pK_a([\text{Fe}(\text{por})(\text{O}_2\text{H}^\bullet)]^+)$ values by our collaborators Dr. Neeraj Kumar and Dr. Simone Rauegi. Both values correlated linearly with the experimental $E_{1/2}$: $\Delta pK_{O_2} = 11(\Delta E_{1/2})$ and $\Delta pK_a([\text{Fe}(\text{por})(\text{O}_2\text{H}^\bullet)]^+) = -28(\Delta E_{1/2})$.¹⁰ Inserting these values and the Brønsted α measured for Fe(por)-catalyzed ORR (0.3) into eq 12 gives eq 13, which predicts a $\log(\text{TOF}_{\text{max}})/\eta_{\text{eff}}$ slope of 19 decades (dec) in TOF_{max} per V in η_{eff} .^{10,15}

$$\begin{aligned} \Delta \log(\text{TOF}_{\text{max}}) &= -\Delta pK_{O_2} + \alpha \Delta pK_a([\text{Fe}(\text{por})(\text{O}_2\text{H}^\bullet)]^+) \\ &[\text{for changes in } E_{1/2}] \end{aligned} \quad (12)$$

$$\begin{aligned} \Delta \log(\text{TOF}_{\text{max}}) &= -(11 + 28\alpha)\Delta E_{1/2} = (-19 \text{ dec/V}) \\ \Delta E_{1/2} &= (19 \text{ dec/V})\Delta\eta_{\text{eff}} \end{aligned} \quad (13)$$

This analysis shows how the electronic structure of the catalyst modulates the barrier for catalysis. Catalysts with more negative $E_{1/2}$ values yield faster TOF_{max} values because O_2 binding is more favorable (larger K_{O_2} and the iron superoxide intermediate is more basic (higher pK_a). The combination of experimental and computational results enabled us to quantitatively interpret the slopes of these intrinsic scaling relationships for a series of catalysts with similar electronic structures.

Effect of Buffer pK_a

A similar scaling relationship can be derived for a set of catalytic systems in which a single Fe(por) catalyst is evaluated using buffers with different pK_a values.¹⁵ Changing the buffer identity shifts the ORR equilibrium potential because higher proton activity makes O_2 reduction more favorable. From the Nernst equation (eq 4 above), each unit decrease in pK_a causes an increase in E_{ORR} by 0.0592 V ($\Delta\eta_{\text{eff}} = -(0.0592 \text{ V})\Delta pK_a$). For the TOF_{max} , a change in the buffer acidity usually only affects the rate of the PT step via the Brønsted law (eq 14; exceptions are described below). This leads to a new scaling relationship (eq 15)

with a predicted scaling slope m of 5.1 dec/V ($\alpha = 0.3$, as above). Figure 6 shows this as the purple line, with experimental results (purple points).¹⁵

$$\Delta \log(\text{TOF}_{\max}) = -\alpha[\Delta \text{p}K_{\text{a}}(\text{HA})] \quad [\text{for changes in HA}] \quad (14)$$

$$\begin{aligned} \alpha[\Delta \text{p}K_{\text{a}}(\text{HA})] &= m(0.0592[\Delta \text{p}K_{\text{a}}(\text{HA})]); \\ m &= (\alpha/0.0592) = (5.1 \text{ dec/V}) \end{aligned} \quad (15)$$

Discussion of $E_{1/2}$ and $\text{p}K_{\text{a}}$ Scaling Relationships

Equations 13 and 15 show that changes in the two key intrinsic properties of the catalytic system, $E_{1/2}$ and buffer $\text{p}K_{\text{a}}$, have very different effects on the scaling slopes. The $\log(\text{TOF}_{\max})/\eta_{\text{eff}}$ relationship is 3.6 times shallower when $\text{p}K_{\text{a}}$ is changed rather than $E_{1/2}$. As a result, can be improved with less penalty to TOF_{\max} by changing the buffer instead of the catalyst identity. For example, replacing $[\text{DMF-H}]^+$ with trifluoroacetic acid ($\text{p}K_{\text{a}} = 6.0$ in DMF) gave a 10^4 increase in TOF_{\max} relative to the predicted value for changing η_{eff} by the same amount via $E_{1/2}$ (Figure 6).¹⁵ The shallow dependence on $\text{p}K_{\text{a}}$ arises because proton transfer is the rate-limiting step, and thus, the proton transfer barrier (G_{PT}^{\ddagger}) changes by only a fraction ($\alpha = 0.3$) of the G_{PT} . In contrast, pre-equilibrium steps will usually be more sensitive to η_{eff} . For example, Wang and Stahl discovered that cobalt-catalyzed O_2 reduction to H_2O_2 showed a shallow $\log(\text{TOF}_{\max})/\eta_{\text{eff}}$ correlation as the catalyst was varied, 6 dec/V versus the 18.5 dec/V we found for Fe(por).²² The origin of this difference was traced to differences in initial O_2 binding. The Fe(por) catalysts have unfavorable KO_2 pre-equilibria that are strongly dependent on $E_{1/2}$. In contrast, O_2 -binding to the cobalt catalysts is strongly favored regardless of $E_{1/2}$. These examples show that there are many possible $\log(\text{TOF}_{\max})/\eta_{\text{eff}}$ scaling relationships, depending on the mechanism of catalysis and the property of the catalytic system being varied.

VII. SCALING RELATIONSHIPS 3: EFFECTS OF CONCENTRATIONS

Molecular scaling relationships can also be derived for the effects of experimental or operational conditions on the catalyst system. The simplest operational choice is the concentrations of the reagents, which includes P_{O_2} , $[\text{HA}]$, $[\text{A}^-]$, and $[\text{H}_2\text{O}]$ for the ORR. Varying each of these parameters influences the $\log(\text{TOF}_{\max})/\eta_{\text{eff}}$ slopes in unique, predictable ways.¹⁵

For changes in concentrations, the slope m of a scaling relationship (eq 5) can be precisely derived from the kinetic and thermodynamic equations (eq 9 and 4, repeated here for ease of presentation).

$$\log(\text{TOF}_{\max}) = m(\eta_{\text{eff}}) + C \quad (5)$$

$$\text{TOF}_{\max} = k_{\text{cat}}[\text{HA}][\text{O}_2] \quad (9)$$

$$E_{\text{O}_2/\text{H}_2\text{O}} = E_{\text{O}_2/\text{H}_2\text{O}}^{\circ} - \frac{2.303RT}{4F} \log \left(\frac{[\text{H}_2\text{O}]^2 [\text{A}^-]^4}{P_{\text{O}_2} [\text{HA}]^4} \right) - (0.0592\text{V})\text{p}K_a \quad (4)$$

Since catalysis is first order in [HA] and P_{O_2} (proportional to $[\text{O}_2]$), a 10-fold increase in either results in a 10-fold increase in TOF. Changing the $[\text{A}^-]$ or $[\text{H}_2\text{O}]$, however, does not influence the TOF, since neither appears in the rate law. 10-fold increases in these concentrations all shift η_{eff} in different ways: +59 mV for [HA], -59 mV for $[\text{A}^-]$, -30 mV for $[\text{H}_2\text{O}]$, and +15 mV for P_{O_2} . Experiments confirm these predictions, as shown by the red and green points (experiments) and lines (theory) in Figure 6.¹⁵ The $\log(\text{TOF}_{\text{max}})/\eta_{\text{eff}}$ slopes for [HA] and P_{O_2} differ by a factor of 4 because [HA] and P_{O_2} contribute equally to the kinetics (eq 9) but have different stoichiometries in the ORR, four HA per O_2 , which set the exponents in the Nernst equation (eq 4).

The ability to predict the relationship between $\log(\text{TOF}_{\text{max}})$ and η_{eff} means that a wide parameter space can be predictably accessed simply by changing the solution conditions for a single catalyst. This conclusion is valuable because most catalysis research involves some searching of parameter space for the best catalytic results (including studies from the authors and those critical of this section³⁴⁻²⁴). Another important use of this $\log(\text{TOF}_{\text{max}})/\eta_{\text{eff}}$ concentration analysis is to enable quantitative comparisons of catalytic systems that were studied under different conditions.

VIII. SCALING RELATIONSHIPS 4: SUMMATIVE EFFECTS

We recently discovered a $\log(\text{TOF}_{\text{max}})/\eta_{\text{eff}}$ scaling relationship with a *negative* slope, using the polycationic iron $\alpha\beta\alpha\beta$ -trimethylanilinium porphyrin (Fe-*o*-TMA) and various carboxylic acid buffers (Figure 7).³⁵ The simultaneous improvement in both TOF_{max} and η_{eff} was unlike all of the scaling relationships above, which had *positive* slopes and involved trade-offs between TOF_{max} and η_{eff} . However, despite seemingly haven “broken” from the scaling relationships, we demonstrated that this unprecedented result could be predicted by combining the known $\text{p}K_a$ and $E_{1/2}$ relationships developed for our Fe(por) systems.

When studied under conditions identical to those of other Fe(por) ORR catalysts (buffered [DMF- H^+]), Fe-*o*-TMA fell close to one of the original $E_{1/2}$ scaling relationships.^{10,35} Thus, the highly cationic ligand did not improve or even affect catalysis, in contrast to what was reported for CO_2 electroreduction.^{25,36} The inverse scaling for Fe-*o*-TMA with buffered carboxylic acids only occurred because the buffer affected both $\text{p}K_a$ and $E_{1/2}$. Buffers with weaker acids (higher $\text{p}K_a$) gave much more negative $E_{1/2}$ values with a roughly linear dependence (Figure 7B). The $E_{1/2}$ shifts were due to axial ligand binding of the anionic carboxylates,^{35,37} an electrostatic effect seen only with anionic ligands and only to the pentacationic catalyst.¹⁵ Because the buffer identity affected both $\text{p}K_a$ and $E_{1/2}$, neither individual scaling relationship predicted the composite changes in the catalytic system. However, by considering changes made to *both* the $\text{p}K_a$ and $E_{1/2}$ components, the individual data points and inverse $\log(\text{TOF}_{\text{max}})/\eta_{\text{eff}}$ correlation could be predicted *quantitatively*.³⁵

$$\begin{aligned}\vec{v}_{\text{p}K_a} &= \langle \Delta\eta_{\text{eff}}, \Delta\log(\text{TOF}_{\text{max}}) \rangle \\ &= \langle -0.059(\Delta\text{p}K_a), -\alpha(\Delta\text{p}K_a) \rangle\end{aligned}\quad (16)$$

$$\begin{aligned}\vec{v}_{E_{1/2}} &= \langle \Delta\eta_{\text{eff}}, \Delta\log(\text{TOF}_{\text{max}}) \rangle \\ &= \langle -\Delta E_{1/2}, -18.5(\Delta E_{1/2}) \rangle\end{aligned}\quad (17)$$

$$\vec{v}_{\text{sum}} = \vec{v}_{\text{p}K_a} + \vec{v}_{E_{1/2}}\quad (18)$$

Using the scaling relations specifically derived for Fe(por)-catalyzed ORR, the *experimental* changes in $\text{p}K_a$ and $E_{1/2}$ in this system were mathematically represented as vectors in the $\log(\text{TOF}_{\text{max}})/\eta_{\text{eff}}$ space (eqs 16 and 17). For instance, the vector in eq 16 describes how changes in $\text{p}K_a$ ($\Delta\text{p}K_a$) affect both η_{eff} and $\log(\text{TOF}_{\text{max}})$ according to the $\text{p}K_a$ relationship described in section VI. An analogous vector exists for changes in $E_{1/2}$ (eq 17). The sum of these two vectors (eq 18) predicts net changes in η_{eff} and $\log(\text{TOF}_{\text{max}})$ using only experimental values for $\text{p}K_a$ and $E_{1/2}$.

For example, replacing $\text{CF}_3\text{C}(\text{O})\text{OH}$ with $\text{CH}_3\text{C}(\text{O})\text{OH}$ gave $\text{p}K_a = 10.9$ and $E_{1/2} = -0.302$. The sum of these changes (eqs 16–18) predicted both the directionality and distance in the observed data: the black + purple vectors sum to the blue vector in Figure 7. This result is a first-of-a-kind application of molecular scaling relationships, where a tandem, two-scaling relationship approach can be used to simultaneously improve both rates and overpotentials.³⁵

We believe that similar vector analyses could be applied to any multistep molecular electrocatalytic reaction where different properties of the catalyst system show different $\log(\text{TOF}_{\text{max}})/\eta_{\text{eff}}$ relationships. This requirement is typically fulfilled because multistep reactions often have pre-equilibrium and rate-limiting steps with different stoichiometries and free energies. Implementing different combinations of these scaling relationships should allow optimization—in some cases via inverse scaling—to achieve faster rates at lower overpotentials.

IX. COUPLING INTRINSIC AND OPERATIONAL PARAMETERS OF A CATALYTIC SYSTEM

The previous sections show how the efficiency of a *catalytic system* can be improved by changing the catalyst and solution conditions. In many of these examples, the “intrinsic” properties of the system (e.g., $E_{1/2}$, $\text{p}K_a$, and catalyst identity) are independent of the “operational” conditions like substrate concentrations.^{15,34} However, the intrinsic and operational parameters cannot always be separated. In the Fe-*o*-TMA system above, the nature and concentration of the buffer affect $E_{1/2}$ via carboxylate binding to the catalyst. The change in catalyst speciation with respect to the solution composition is what enables inverse scaling.³⁵

Another example occurs when a catalyst's ligand contains protonatable functionalities such that changes to acid concentration (an operational parameter) can influence the intrinsic properties of the catalyst. For instance, our studies of the ORR catalyzed by iron tetra-*o*-pyridylporphyrin showed an unusual, inverse-order dependence on [DMF-H⁺].¹⁰ The decrease in TOF_{max} occurred in tandem with an 88 mV shift in $E_{1/2}$ per decade increase in [DMF-H⁺], which was attributed to protonation equilibria among the many proteomers (Figure 8). The increase in $E_{1/2}$ caused decreases in both K_{O_2} and the basicity of the superoxide adduct. Because variation in acid concentration, an operational parameter, changes the intrinsic *catalyst identity*, the two parameters are inherently connected and must be considered together when analyzing log(TOF_{max})/ η_{eff} relationships.

Many other electrocatalytic systems likely exhibit similar complex relationships between intrinsic and operational parameters. It is therefore more valuable to consider globally how all solution components affect catalyst behavior. The alternative approach, which emphasizes only standard state conditions, can miss these cooperative effects. In addition, measurements and extrapolations to standard states are challenging and are in practice almost never done (even by those who advocate for such an approach^{24,25}). We emphasize that the linkage between various parameters of a catalytic system is not a complication but rather *an opportunity*. Cooperativity between the catalyst active site and surrounding medium is an exciting, underexplored approach to improving catalysis.

X. CONCLUSIONS AND PROSPECTS

This Account surveys our examination of oxygen reduction reaction (ORR) catalysis by soluble iron porphyrins (Fe(por)) in organic solvents, which builds from a fundamental understanding of the reaction thermodynamics, kinetics, and mechanism. We developed procedures to determine nonaqueous standard potentials for the ORR and other PCET half reactions, and we examined the rate law and mechanism of Fe(por)-catalyzed ORR using both electrochemical and spectroscopic techniques. Key reaction intermediates were identified and their thermochemistry measured. Examining our large data set of turnover frequencies and thermochemical overpotentials (η_{eff}) revealed a number of empirical linear correlations, $\log(\text{TOF}_{\text{max}}) = m(\eta_{\text{eff}}) + C$, when one component of the catalytic system is changed.

Such “molecular scaling relationships” have been found in several reactions, including H₂ evolution and O₂ reduction to water or hydrogen peroxide,^{10,14,22,27,35,38} and could be further developed for any multiproton/multielectron catalysis. Deriving relationships between log(TOF_{max}) and η_{eff} requires knowing the rate law for catalysis and the thermodynamics of the reaction of interest. For operational parameters like substrate concentration, the reaction order in substrate and the stoichiometry of that substrate in the overall reaction dictate the slope of the scaling line. Molecular scaling relationships based on intrinsic properties like catalyst $E_{1/2}$ and buffer pK_a require additional experimental or computational inputs.

These connections between kinetics and thermodynamics require linear free energy relationships (LFERs). LFERs, while approximate, have been shown experimentally and

computationally to hold for many reaction steps and are key to both molecular scaling relationships and heterogeneous analogues. They assume (i) that the free energies of intermediates scale with each other, here the linear scaling of both pK_{O_2} and $pK_a([Fe(por)(O_2H^*)])^+$ with $E_{1/2}$, and (ii) that G^\ddagger for each step correlates with the G° for that step, here in the Brønsted catalysis “law” relating k_{PT} to G^\ddagger_{PT} .

Electrocatalysis by soluble molecules is often found to follow mechanisms in which PT and ET occur in *separate* steps of the cycle. Therefore, changing one component of a catalytic system affects the different steps of the cycle in different ways, and a single scaling parameter cannot provide a complete description. The TOF_{max} for Fe(por)-catalyzed ORR responds very differently when the η_{eff} is varied via the buffer pK_a , which usually affects only the rate-limiting PT step, rather than by changing the catalyst $E_{1/2}$ which affects that step *and* the pre-equilibrium ET and O_2 -binding steps. In contrast, the mechanisms typically used for heterogeneous PCET scaling relationships involve e^-/H^+ addition together, so that the energetics of each step usually correlate with the overall energetics of the multiproton/multielectron reactions, allowing the use of a single scaling parameter such as a surface–H bond strength. For molecular electrocatalysis, using η_{eff} is advantageous as the thermochemical parameter because it considers contributions from multiple system components, and because it is a critical parameter to be optimized.

Molecular scaling relationships are powerful tools for understanding and improving molecular electrocatalytic processes. They predict behavior across a wide range of parameter space, thus enabling comparisons of catalytic systems examined under different conditions. The molecular scaling relationships developed here reveal underlying thermochemical insights about a catalytic system under any conditions, even when standard states are challenging to define. These molecular scaling relationships often can *predict* reactivity under a variety of conditions and with different catalysts. Most notably, these scaling relationships *quantitatively* explain the dramatic improvement in ORR electrocatalysis when using a highly cationic iron porphyrin with buffers containing carboxylic acid buffers. This improvement results from cooperativity between the nominal catalyst and the other components of the catalytic system, emphasizing that both intrinsic and operational parameters must be included in analyses of electrocatalytic processes.

We hope that this Account will encourage other researchers in the field to use this approach for their systems. Once the thermochemistry and rate law have been established, molecular scaling relationships can be readily derived and used for understanding and improving catalytic performance.

ACKNOWLEDGMENTS

The authors thank all our co-workers, colleagues, and collaborators who contributed to this work. This research was supported as part of the Center for Molecular Electrocatalysis, an Energy Frontier Research Center funded by the U.S. Department of Energy, Office of Science, Office of Basic Energy Sciences. D.J.M. recognizes support from an NSF GRFP. M.L.P. recognizes current support by a NIH postdoctoral fellowship (F32GM130071).

Biographies

Daniel J. Martin received his B.S. in Chemistry with Highest Honors from The University of North Carolina at Chapel Hill in 2015. He is currently a Ph.D. candidate at Yale University as an NSF Graduate Research Fellow.

Catherine F. Wise received a B.S. in Chemistry from the College of William and Mary in 2015 and is currently a Ph.D. Candidate in the Department of Chemistry at Yale University.

Michael L. Pegis received his B.S. from Western Washington University and his Ph.D. in Chemistry from Yale University. He is currently an NIH postdoctoral fellow in the Surendranath group at MIT.

James M. Mayer did undergraduate research at Hunter College with Edwin Abbott, and with William Klemperer while earning his A.B. at Harvard. He completed a Ph.D. at Caltech under the direction of John Bercaw in 1982, and after two years as a Visiting Scientist at DuPont, he moved to the University of Washington. In 2014, he moved to Yale University.

REFERENCES

- (1). Solomon EI; Stahl SS, Introduction: Oxygen Reduction and Activation in Catalysis. *Chem. Rev* 2018, 118, 2299–2301. [PubMed: 29534575]
- (2). Wikström M; Krab K; Sharma V. Oxygen Activation and Energy Conservation by Cytochrome c Oxidase. *Chem. Rev* 2018, 118, 2469–2490. [PubMed: 29350917]
- (3). Mano N; de Poulpique A. O₂ Reduction in Enzymatic Biofuel Cells. *Chem. Rev* 2018, 118, 2392–2468. [PubMed: 28930449]
- (4). Gewirth AA; Varnell JA; DiAscro AM Nonprecious Metal Catalysts for Oxygen Reduction in Heterogeneous Aqueous Systems. *Chem. Rev* 2018, 118, 2313–2339. [PubMed: 29384375]
- (5). Kulkarni A; Siahrostami S; Patel A; Nørskov JK, Understanding Catalytic Activity Trends in the Oxygen Reduction Reaction. *Chem. Rev* 2018, 118, 2302–2312. [PubMed: 29405702]
- (6). Montemore MM; van Spronsen MA; Madix RJ; Friend CM O₂ Activation by Metal Surfaces: Implications for Bonding and Reactivity on Heterogeneous Catalysts. *Chem. Rev* 2018, 118, 2816–2862. [PubMed: 29116787]
- (7). Pegis ML; Wise CF; Martin DJ; Mayer JM Oxygen Reduction by Homogeneous Molecular Catalysts and Electrocatalysts. *Chem. Rev* 2018, 118, 2340–2391. [PubMed: 29406708]
- (8). Ren S; Joulié D; Salvatore D; Torbensen K; Wang M; Robert M; Berlinguette CP Molecular Electrocatalysts Can Mediate Fast, Selective CO₂ Reduction in a Flow Cell. *Science* 2019, 365, 367–369. [PubMed: 31346062]
- (9). Passard G; Ullman AM; Brodsky CN; Nocera DG Oxygen Reduction Catalysis at a Dicobalt Center: The Relationship of Faradaic Efficiency to Overpotential. *J. Am. Chem. Soc* 2016, 138, 2925–2928. [PubMed: 26876226]
- (10). Pegis ML; McKeown BA; Kumar N; Lang K; Wasylenko DJ; Zhang XP; Raugei S; Mayer JM Homogenous Electrocatalytic Oxygen Reduction Rates Correlate with Reaction Overpotential in Acidic Organic Solutions. *ACS Cent. Sci* 2016, 2, 850–856. [PubMed: 27924314]
- (11). Rountree ES; McCarthy BD; Eisenhart TT; Dempsey JL Evaluation of Homogeneous Electrocatalysts by Cyclic Voltammetry. *Inorg. Chem* 2014, 53, 9983–10002. [PubMed: 25247280]
- (12). Appel AM; Helm ML Determining the Overpotential for a Molecular Electrocatalyst. *ACS Catal.* 2014, 4, 630–633.
- (13). Costentin C; Drouet S; Robert M; Savéant J-M Turnover Numbers, Turnover Frequencies, and Overpotential in Molecular Catalysis of Electrochemical Reactions. *Cyclic Voltammetry and Preparative-Scale Electrolysis. J. Am. Chem. Soc* 2012, 134, 11235–11242. [PubMed: 22670885]

- Author Manuscript
- Author Manuscript
- Author Manuscript
- Author Manuscript
- (14). Costentin C; Passard G; Savéant J-M Benchmarking of Homogeneous Electrocatalysts: Overpotential, Turnover Frequency, Limiting Turnover Number. *J. Am. Chem. Soc* 2015, 137, 5461–5467. [PubMed: 25757058]
 - (15). Pegis ML; Wise CF; Koronkiewicz B; Mayer JM Identifying and Breaking Scaling Relations in Molecular Catalysis of Electrochemical Reactions. *J. Am. Chem. Soc* 2017, 139, 11000–11003. [PubMed: 28724290]
 - (16). Roberts JAS; Bullock RM Direct Determination of Equilibrium Potentials for Hydrogen Oxidation/Production by Open Circuit Potential Measurements in Acetonitrile. *Inorg. Chem* 2013, 52, 3823–3835. [PubMed: 23488870]
 - (17). Pegis ML; Roberts JAS; Wasylenko DJ; Mader EA; Appel AM; Mayer JM Standard Reduction Potentials for Oxygen and Carbon Dioxide Couples in Acetonitrile and N, N'-Dimethylformamide. *Inorg. Chem* 2015, 54, 11883–11888. [PubMed: 26640971]
 - (18). Lindley BM; Appel AM; Krogh-Jespersen K; Mayer JM; Miller AJM Evaluating the Thermodynamics of Electrocatalytic N₂ Reduction in Acetonitrile. *ACS Energy Lett.* 2016, 1, 698–704.
 - (19). Hooe SL; Rheingold AL; Machan CW Electrocatalytic Reduction of Dioxygen to Hydrogen Peroxide by a Molecular Manganese Complex with a Bipyridine-Containing Schiff Base Ligand. *J. Am. Chem. Soc* 2018, 140, 3232–3241. [PubMed: 29216711]
 - (20). Fourmond V; Jacques P-A; Fontecave M; Artero V. H₂ Evolution and Molecular Electrocatalysts: Determination of Overpotentials and Effect of Homoconjugation. *Inorg. Chem* 2010, 49, 10338–10347. [PubMed: 20964310]
 - (21). Nichols EM; Derrick JS; Nistanaki SK; Smith PT; Chang CJ Positional Effects of Second-Sphere Amide Pendants on Electrochemical CO₂ Reduction Catalyzed by Iron Porphyrins. *Chem. Sci* 2018, 9, 2952–2960. [PubMed: 29732079]
 - (22). Wang Y-H; Pegis ML; Mayer JM; Stahl SS Molecular Cobalt Catalysts for O₂ Reduction: Low-Overpotential Production of H₂O₂ and Comparison with Iron-Based Catalysts. *J. Am. Chem. Soc* 2017, 139, 16458–16461. [PubMed: 29039921]
 - (23). Kilgore UJ; Stewart MP; Helm ML; Dougherty WG; Kassel WS; DuBois MR; DuBois DL; Bullock RM Studies of a Series of [Ni(P^R₂N^{Ph}₂)₂(CH₃CN)]²⁺ Complexes as Electrocatalysts for H₂ Production: Substituent Variation at the Phosphorus Atom of the P₂N₂ Ligand. *Inorg. Chem* 2011, 50, 10908–10918. [PubMed: 21999814]
 - (24). Costentin C; Drouet S; Robert M; Savéant J-M A Local Proton Source Enhances CO₂ Electroreduction to CO by a Molecular Fe Catalyst. *Science* 2012, 338, 90–94. [PubMed: 23042890]
 - (25). Azcarate I; Costentin C; Robert M; Savéant J-M Through-Space Charge Interaction Substituent Effects in Molecular Catalysis Leading to the Design of the Most Efficient Catalyst of CO₂-to-CO Electrochemical Conversion. *J. Am. Chem. Soc* 2016, 138, 16639–16644. [PubMed: 27976580]
 - (26). Klug CM; Cardenas AJP; Bullock RM; O'Hagan M; Wiedner ES Reversing the Tradeoff between Rate and Overpotential in Molecular Electrocatalysts for H₂ Production. *ACS Catal.* 2018, 8, 3286–3296.
 - (27). Quaino P; Juarez F; Santos E; Schmickler W. Volcano Plots in Hydrogen Electrocatalysis - Uses and Abuses. *Beilstein J. Nanotechnol* 2014, 5, 846–854. [PubMed: 24991521]
 - (28). Greeley J; Jaramillo TF; Bonde J; Chorkendorff I; Nørskov JK Computational High-Throughput Screening of Electrocatalytic Materials for Hydrogen Evolution. *Nat. Mater* 2006, 5, 909–913. [PubMed: 17041585]
 - (29). Trasatti S. Work Function, Electronegativity, and Electrochemical Behaviour of Metals. *J. Electroanal. Chem. Interfacial Electrochem* 1972, 39, 163–184.
 - (30). Pegis ML; Martin DJ; Wise CF; Brezny AC; Johnson SI; Johnson LE; Kumar N; Raugi S; Mayer JM Mechanism of Catalytic O₂ Reduction by Iron Tetraphenylporphyrin. *J. Am. Chem. Soc* 2019, 141, 8315–8326. [PubMed: 31042028]
 - (31). Wasylenko DJ; Rodriguez C; Pegis ML; Mayer JM Direct Comparison of Electrochemical and Spectrochemical Kinetics for Catalytic Oxygen Reduction. *J. Am. Chem. Soc* 2014, 136, 12544–12547. [PubMed: 25137524]

- (32). Costentin C; Savéant J-M Multielectron, Multistep Molecular Catalysis of Electrochemical Reactions: Benchmarking of Homogeneous Catalysts. *ChemElectroChem* 2014, 1, 1226–1236.
- (33). Hoops S; Sahle S; Gauges R; Lee C; Pahle J; Simus N; Singhal M; Xu L; Mendes P; Kummer U. COPASI-a COMplex PATHway Simulator. *Bioinformatics* 2006, 22, 3067–3074. [PubMed: 17032683]
- (34). Costentin C; Savéant J-M Homogeneous Molecular Catalysis of Electrochemical Reactions: Manipulating Intrinsic and Operational Factors for Catalyst Improvement. *J. Am. Chem. Soc* 2018, 140, 16669–16675. [PubMed: 30392356]
- (35). Martin DJ; Mercado BQ; Mayer JM Combining Scaling Relationships Overcomes Rate versus Overpotential Trade-Offs in O₂ Molecular Electrocatalysis. *Sci. Adv* 2020, 6, No. eaaz3318.
- (36). Nichols AW; Machan CW Secondary-Sphere Effects in Molecular Electrocatalytic CO₂ Reduction. *Front. Chem* 2019, 7, 1–19. [PubMed: 30778383]
- (37). Lexa D; Rentien P; Savéant JM; Xu F. Methods for Investigating the Mechanistic and Kinetic Role of Ligand Exchange Reactions in Coordination Electrochemistry. *J. Electroanal. Chem. Interfacial Electrochem* 1985, 191, 253–279.
- (38). Wang Y-H; Schneider PE; Goldsmith ZK; Mondal B; Hammes-Schiffer S; Stahl SS Brønsted Acid Scaling Relationships Enable Control Over Product Selectivity from O₂ Reduction with a Mononuclear Cobalt Porphyrin Catalyst. *ACS Cent. Sci* 2019, 5, 1024–1034. [PubMed: 31263762]

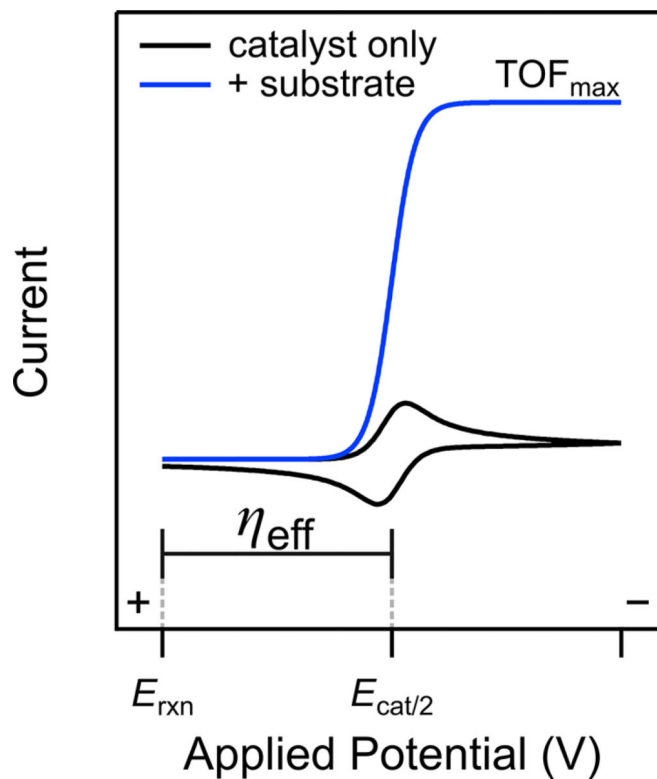
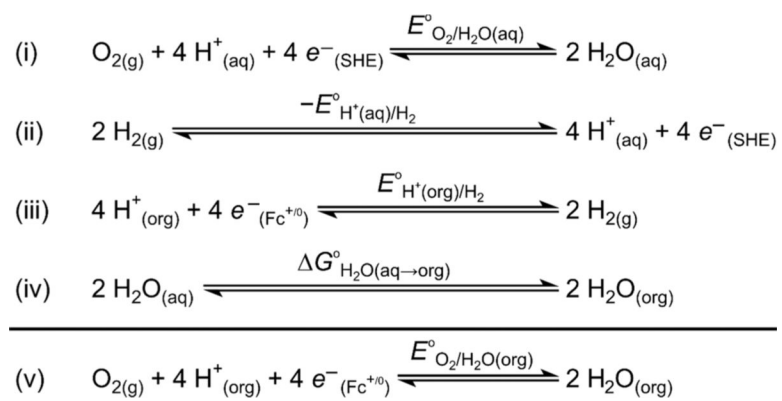
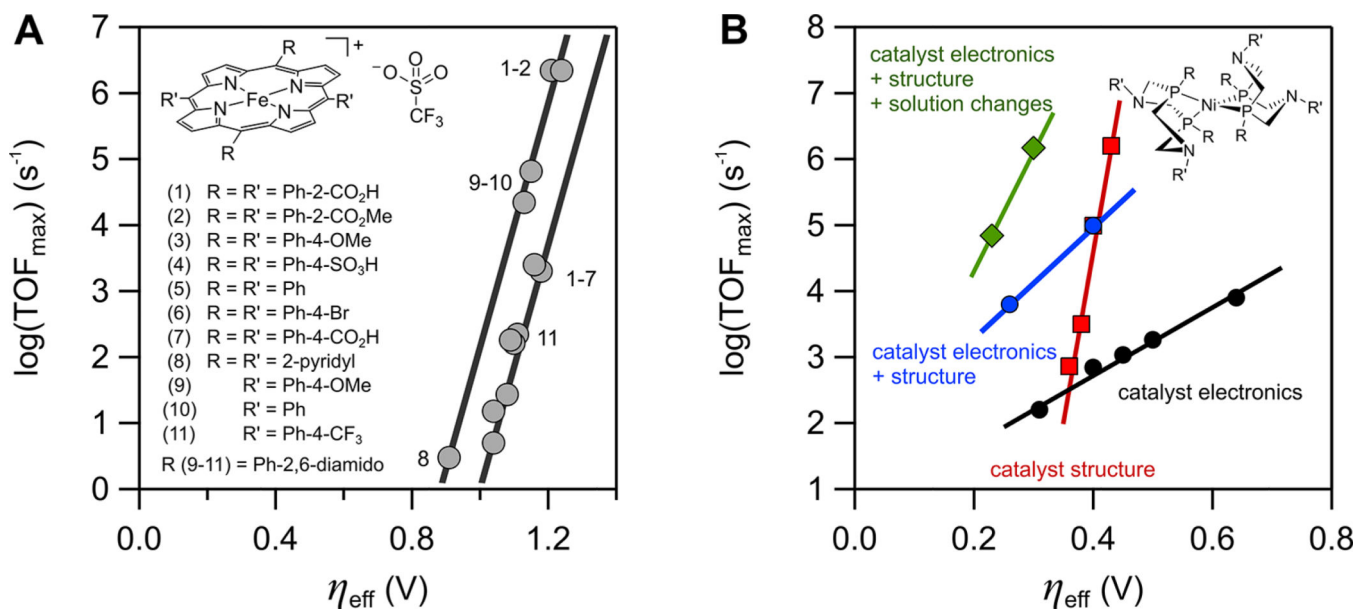


Figure 1. Simulated voltammograms of an electrocatalytic (EC') reaction driven by a molecular catalyst in the presence (blue) and absence (black) of substrate. E_{rxn} is the equilibrium potential of the catalyzed reaction, and $E_{\text{rxn}} - E_{\text{cat}/2}$ is the reaction overpotential (η_{eff}). Adapted with permission from ref 7. Copyright 2018 American Chemical Society.

**Scheme 1.**

Thermochemical Cycle to Estimate $E^\circ_{\text{O}_2/\text{H}_2\text{O}}$ in Nonaqueous Solvents from $E^\circ_{\text{H}^+/\text{H}_2}$ ^a

^aAdapted from ref 17.

**Figure 2.**

Plots of $\log(\text{TOF}_{\text{max}})$ vs η_{eff} : (A) For the ORR catalyzed by various Fe(por) complexes with DMF-H⁺ in MeCN and DMF (some catalysts [inset] were studied in both solvents; see ref 10). (Adapted with permission from ref 10. Copyright 2016 American Chemical Society.)

(B) For catalytic hydrogen evolution by a series of structurally similar nickel phosphine-amine complexes. The lines describe scaling relationships between TOF_{max} and η_{eff} . (Adapted with permission from ref 26. Copyright 2018 American Chemical Society.)

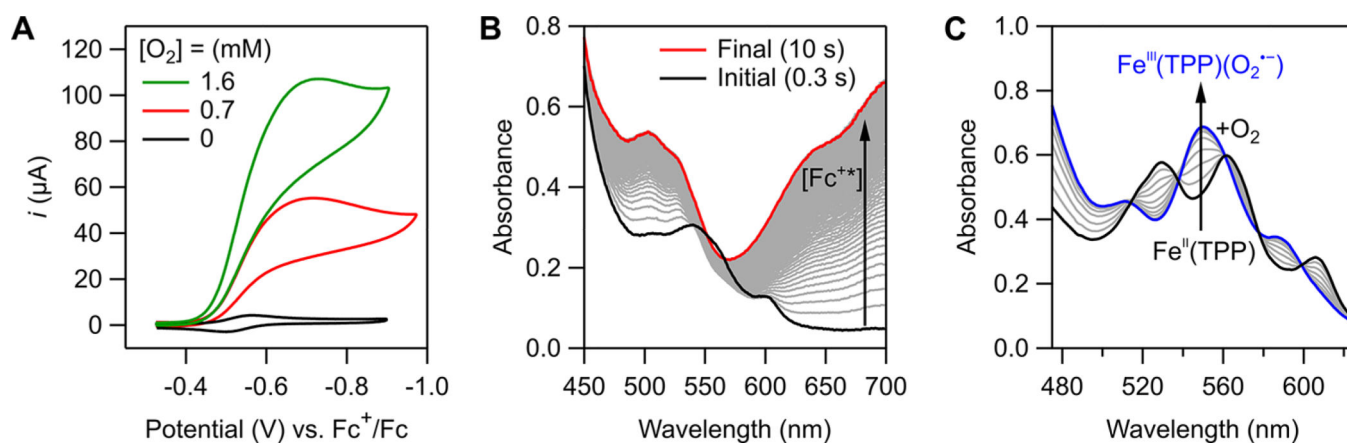


Figure 3.

(A) Voltammograms of 0.3 mM $[\text{Fe}^{\text{III}}(\text{TPP})]\text{OTf}$ in the presence of 1 M $p\text{TsOH}$ and varying $[\text{O}_2]$. (B) Stopped-flow optical spectra for the reaction of O_2 (0.33 mM), $p\text{TsOH}$ (50 mM), and Fc^* (3 mM) catalyzed by $[\text{Fe}^{\text{III}}(\text{TPP})]\text{OTf}$ (30 μM), showing the formation of Fc^{*+} (arrow). (C) Optical spectra of a titration of O_2 -saturated DMF into a solution of 50 μM $\text{Fe}^{\text{II}}(\text{TPP})$ and 0.1 M $[n\text{-Bu}_4\text{N}][\text{PF}_6]$ at 213 K. Figures adapted with permission from ref 30. Copyright 2019 American Chemical Society.

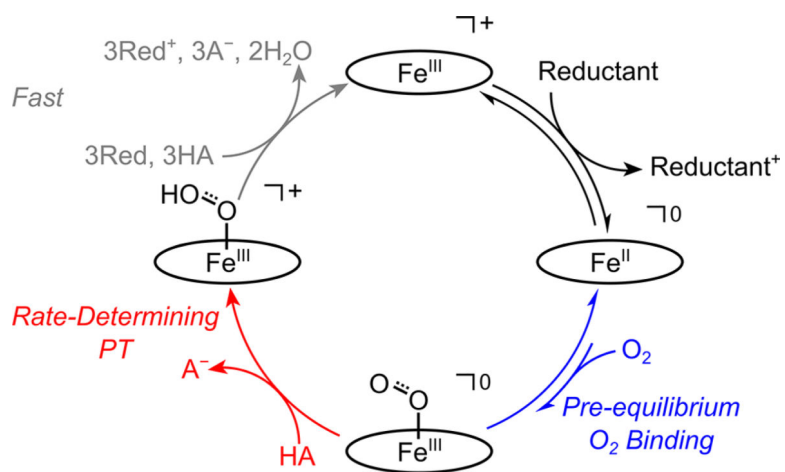


Figure 4. General mechanism for O_2 reduction catalyzed by $\text{Fe}(\text{por})$ in DMF or MeCN, with the porphyrin abbreviated as an oval. “Reductant” can be either a chemical reductant or an electrode. Adapted with permission from ref 30. Copyright 2019 American Chemical Society.

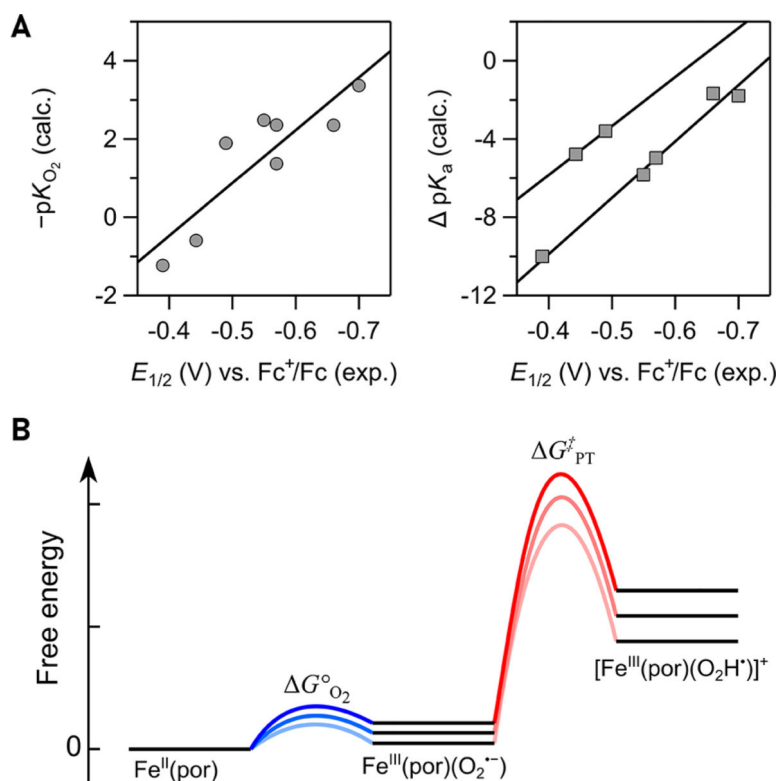


Figure 5.

(A) Computed values for O_2 binding (pK_{O_2} , left) and $pK_a[Fe^{III}(por)(O_2H^*)]^+ - pK_a[DMF-H]^+$ (right), correlated with $E_{1/2}(Fe^{III}/Fe^{II})$ for some of the $Fe(por)$ in Figure 2A (ref 10). (B) Chemical steps to the rate-determining step and their free energy profile for three different $Fe(por)$ catalysts, equivalent to eq 10. Adapted with permission from ref 10. Copyright 2016 American Chemical Society.

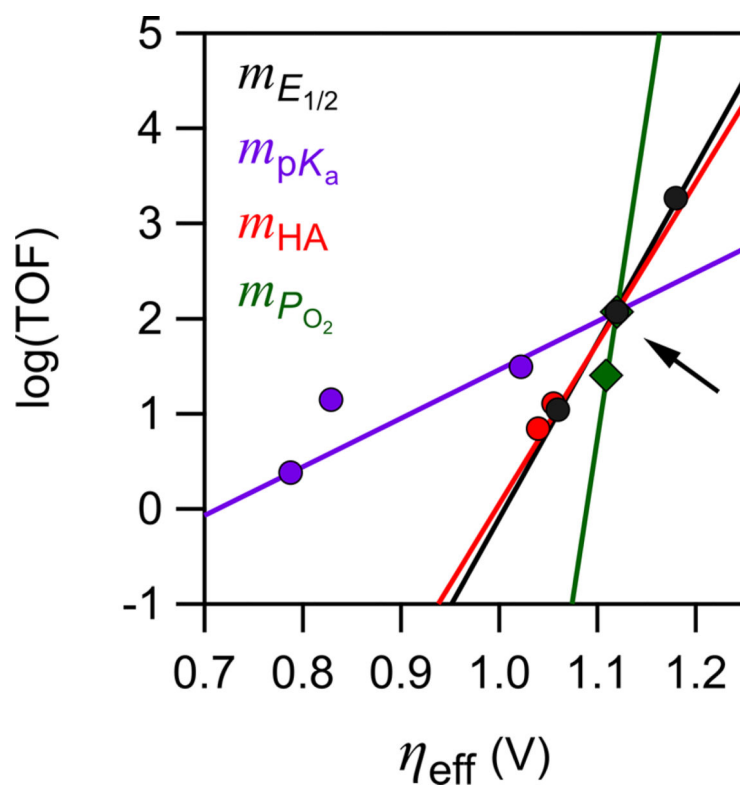


Figure 6. Scaling relations for Fe(por) ORR catalysis predicted (lines) and measured (points) upon changing the acid concentration (red), partial pressure of O₂ (green), acid pK_a (purple), and catalyst E_{1/2} (black; additional data points shown in Figure 2A). The intersection point (arrow) is Fe(TPP)OTf with 100 mM H–DMF⁺ under 1 atm of O₂. Adapted with permission from ref 15. Copyright 2017 American Chemical Society.

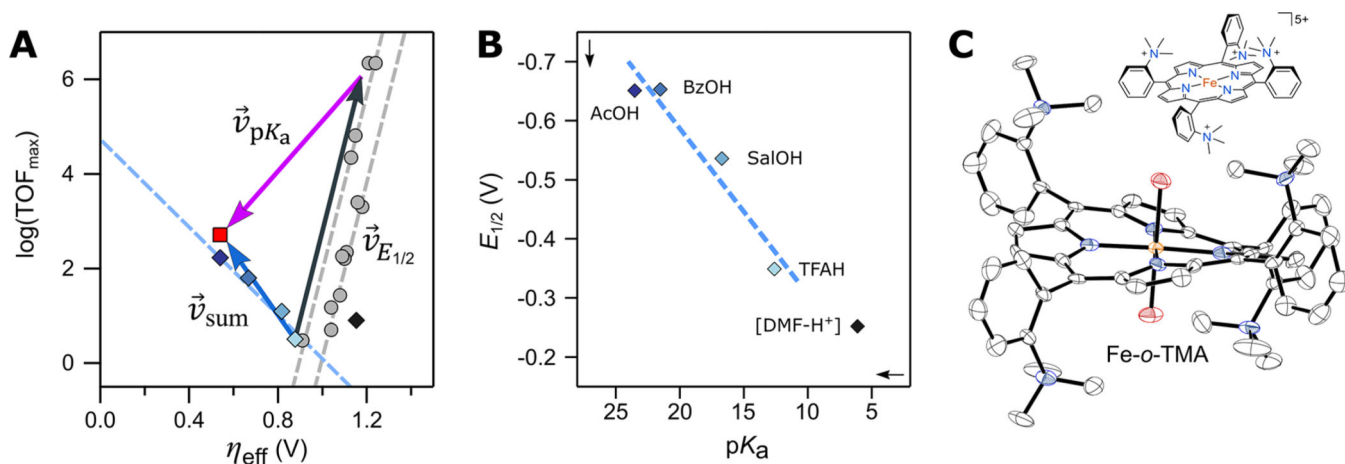


Figure 7.

(A) Plot of $\log(\text{TOF}_{\text{max}})$ vs η_{eff} for catalytic systems of Fe-*o*-TMA and varying buffers (blue diamonds match buffers in part B). Superimposed vectors show predicted changes from $\text{p}K_a$ (purple), $E_{1/2}$ (black), and summative effects (blue). The predicted/observed values for acetic acid buffer are the red square/dark-blue diamond. Prior Fe(por) data and $E_{1/2}$ scaling relationships included for reference (gray). (B) Plot of $E_{1/2}$ vs acid $\text{p}K_a$ at 0.1 M buffer. (C) Drawing of Fe-*o*-TMA and the solid-state X-ray crystal structure of [Fe-*o*-TMA·2H₂O]OTf₅ (H atoms and triflates omitted, thermal ellipsoids at 50% probability). Figures adapted with permission from ref 35. Copyright 2020 American Association for the Advancement of Science.

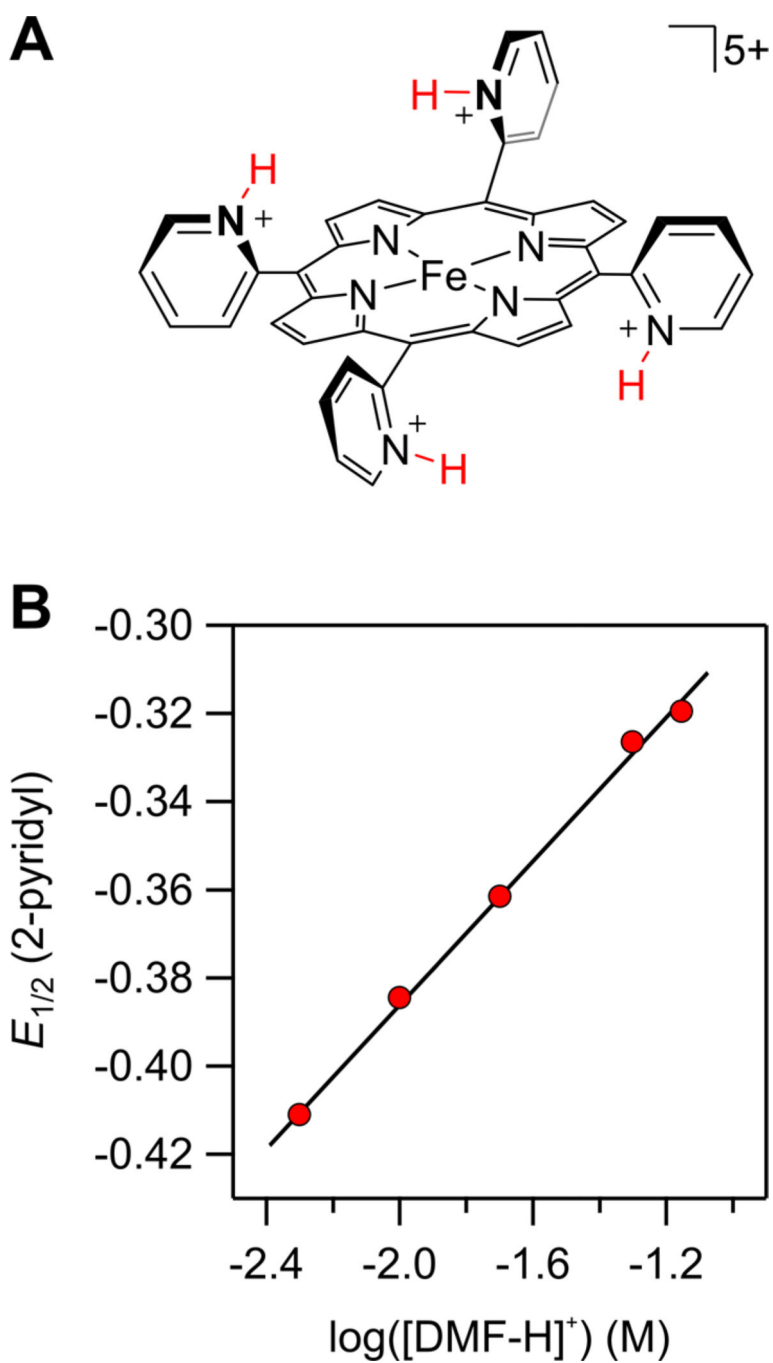


Figure 8. Iron *o*-pyridylporphyrin, shown as the tetra-protonated complex, and its $E_{1/2}$ as a function of [HA]. Adapted with permission from ref 10. Copyright 2016 American Chemical Society.